MATERIALS CHEMISTRY FRONTIERS

RESEARCH ARTICLE

View Article Online
View Journal | View Issue

Cite this: *Mater. Chem. Front.*, 2022, **6**, 1803

Spiro-configured dibenzosuberene compounds as deep-blue emitters for organic light-emitting diodes with a CIE*y* of 0.04†

Clément Brouillac, [a] Wan-Shan Shen,[b] Joëlle Rault-Berthelot, [a] Olivier Jeannin,[a] Cassandre Quinton, [a] Zuo-Quan Jiang [b] and Cyril Poriel [a]*[a]

Received 31st March 2022,
Accepted 13th May 2022

DOI: 10.1039/d2qm00287f

rsc.li/frontiers-materials

Deep blue electroluminescence is highly required for organic light-emitting diode (OLED) technology. However, designing fluorophores displaying adequate CIE coordinates and particularly a low CIE*y* is far from an easy task. We report in this work the synthesis, the physico-chemical properties and the application of deep blue emitters constructed using the dibenzosuberene (DBS) molecular fragment in OLEDs. Three emitters, **SPA-DBS**, **SIA-DBS** and **SQPTZ-DBS**, have been constructed following a similar molecular design strategy that is the *spiro* connection of an electron rich unit, namely *N*-phenylacridine (PA), indoloacridine (IA) or quinolinophenothiazine (QPTZ) to the DBS core. The PA, IA and QPTZ fragments are known to be efficient hole injecters due to their strong electron-rich character. Through a structure/property relationship study, we analyse the electrochemical, photophysical and thermal behaviours of these three emitters. When used as an emitter in an OLED, a deep-blue emission with CIE of (0.16, 0.04) is obtained with **SPA-DBS**, reaching an EQE of *ca*. 1% and a V_{on} of 4 V. The CIE*y* coordinate of 0.04 appears to be particularly low and fits the NSTC, ITU and EBU standards.

Introduction

In the past three decades, organic light-emitting diode (OLED) technology has witnessed a fantastic development and is now released in the market.[1–3] The efforts of chemists, physicists, and materials scientists have led to achieving very high efficiency OLEDs. From many aspects, the technology has significantly evolved since the pioneering studies of Tang in 1987.[4] One of the most important features is undoubtedly the different generations of emitters, which have been used to improve the device performance from fluorescent materials (Generation I)[5–7] to phosphorescent materials (Generation II)[8–13] and to thermally activated delayed fluorescent materials (Generation III).[14,15] Achieving an efficient emission on both ends of the visible spectrum *i.e.*, the violet[16–19] and near-infrared[20] regions, has always been a major challenge in this field. These wavelengths can open up novel applications for future OLEDs. For example, a light source with a wavelength of 405 nm is particularly awaited as a variety of bacteria are sensible to this wavelength (antibacterial blue light).[21] Efficient and stable emission in the violet/deep blue region has always been an important field of research in the OLED technology.[5,12,22–25] However, whatever the nature of the emitters, achieving high efficiency OLEDs in this range of wavelengths has been one of the most difficult problems to solve for the last twenty years. For example, in phosphorescent OLEDs, which are the most mature technology in the field, very high efficiency red, green and sky-blue devices have been achieved (EQE above 25%)[13,22–27] but deep blue and violet OLEDs are still unattainable. In terms of CIE coordinates, different standards can be found in the literature. According to the National Television Standards Committee (NTSC) standard, the Commission Internationale de l'Eclairage (CIE) color coordinates for pure blue light are x = 0.14 and y = 0.08. The y coordinate is even lower by the recommendations of the European Broadcasting Union (EBU) (x = 0.15/y = 0.06)[24,28] and the International Telecommunication Union (ITU) (ITU-R Recommendation BT.2020: x = 0.131/y = 0.046).[29] Achieving these CIE coordinates in an OLED is far from an easy task, especially the CIE*y*, and needs very precise molecular designs of the emissive layer. The challenge of deep-blue emitting OLEDs mainly lies in the difficulty of achieving efficient emitters fulfilling all the desired characteristics.

[a] *Univ Rennes, CNRS, ISCR-UMR CNRS 6226, F-35000 Rennes, France. E-mail: cyril.poriel@univ-rennes1.fr*
[b] *Institute of Functional Nano & Soft Materials (FUNSOM), Jiangsu Key Laboratory for Carbon-Based Functional Materials & Devices, Soochow University, Suzhou, Jiangsu 215123, China*

† Electronic supplementary information (ESI) available: Materials synthesis, their thermal, photophysical and electrochemical properties, theoretical modeling and device data. CCDC 2149596 (**SPA-DBS**) and 2149597 (**SIA-DBS**). For ESI and crystallographic data in CIF or other electronic format see DOI: **https://doi.org/10.1039/d2qm00287f**

Indeed, a deep-blue emitter should have a wide bandgap (>3 eV), which is detrimental for charge injection within an OLED device. Incorporation of electron-rich (electron donor) and electron-poor (electron acceptor) units in the molecular structure is an interesting strategy to reduce the carrier injection barrier with a better fit with the electrode Fermi levels. However, the incorporation of donor and acceptor functional units can lead to a red shift of the emission wavelength due to intramolecular charge transfer (ICT). In order to avoid this red shift, the molecular construction should separate the emitter from the charge injection group. In addition, the emission in the solid state should be efficient and not be shifted compared to the solution as often observed when π–π interactions occur.[28] As the study of elementary building units has been one of the driving forces of organic electronics for the last thirty years, we wish to report herein a barely studied molecular fragment, in the field of blue emitters, that is dibenzosuberene (DBS).[30–32] DBS is a double bridged biphenyl unit with one double bond on one side and a methylene unit on the other. There is a clear analogy between this fragment and the widely known fluorene fragment in which the double bond is replaced by a direct carbon–carbon bond.

Herein, three emitters, **SPA-DBS**, **SIA-DBS** and **SQPTZ-DBS**, have been constructed following a similar molecular design strategy that is the *spiro* connection of an electron-rich unit, namely *N*-phenylacridine (PA),[33–35] indoloacridine (IA)[36] or quinolinophenothiazine (QPTZ)[37–39] to the DBS core. The PA, IA and QPTZ fragments are known to be efficient hole injecters due to their strong electron-rich character; in other words they possess high HOMO levels. On the other hand, the *spiro* connection is known to be a very efficient structural feature to improve the thermal and morphological properties and also allows controlling the interactions between the two orthogonal functional units.[3,40–43] In this work, we report the synthesis, the physico-chemical properties and the application of three blue emitters based on the DBS core in OLEDs. In the solid state, these emitters display an emission in the deep-blue region. When used as an emitter in an OLED, a blue emission with CIE coordinates of (0.16, 0.04) is obtained with **SPA-DBS**, reaching an EQE of *ca*. 1% and possessing a y CIE coordinate below 0.1, fitting the NSTC, ITU and EBU standards.

Synthesis

When designing an organic semi-conductor for electronics, thinking about its synthetic approach is a mandatory step.[43,44] The present target molecules have been synthesized at the multi-gram scale, from commercially available starting material dibenzosuberenone **1**, through an efficient two-step approach (Scheme 1). The nucleophilic addition reaction of dibenzosuberenone with the corresponding lithiated intermediate derivatized from PA (**2**), IA (**3**) or QPTZ (**4**) was first

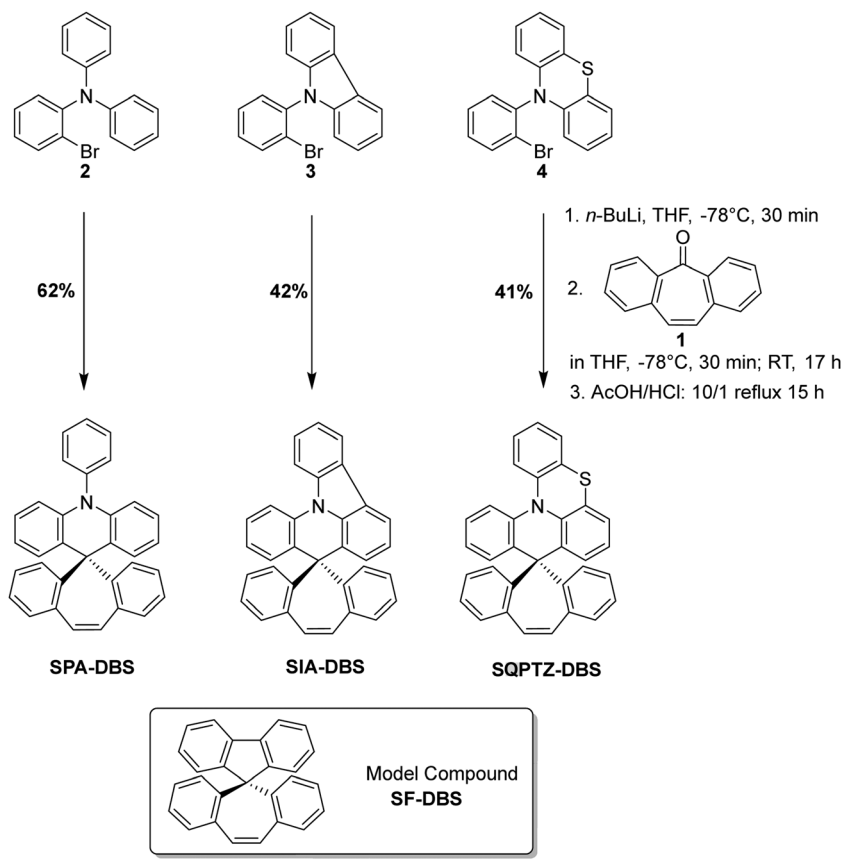

Scheme 1 Synthesis of **SPA-DBS**, **SIA-DBS** and **SQPTZ-DBS**.

performed. Electrophilic intramolecular cyclization of the resulting suberenol (not isolated) in acidic media (HCl/AcOH) afforded the corresponding materials with 62% yield for **SPA-DBS**, 42% yield for **SIA-DBS** and 41% yield for **SQPTZ-DBS**. Thus, this synthetic approach is short, efficient and low cost as it uses cheap starting materials (less than 5 € per g for both **SIA-DBS** and **SQPTZ-DBS** and 8 € per g for **SPA-DBS**) and no palladium catalyst. In order to precisely study the impact of the association of the electron-rich fragments with the DBS core, a model compound will also be studied, namely dibenzosuberene-fluorene **SF-DBS**.

Structural properties

SPA-DBS (CCDC 2149596) and **SIA-DBS** (CCDC 2149597) have been crystallised by vapour diffusion of pentane in $CDCl_3$ in order to confirm their molecular structure by X-ray crystallography and to study the structural characteristics (see X-ray data in the ESI†). Unfortunately, despite intensive scouting, it was not possible to grow crystals of **SQPTZ-DBS**. Opposite to the two others, this compound does not display any crystallization transition phase as observed in DSC (see Fig. 6). **SPA-DBS** crystallizes in an orthorhombic system, $P2_12_12_1$ containing two molecules (see Fig S18 in ESI†). **SIA-DBS** crystallizes in a monoclinic system, $P2_1/c$ (see Fig. S19 in ESI†). In the two molecules, the PA or IA unit and the DBS unit are almost orthogonal with a twist angle (value in orange in Fig. 1) of 90° for **SPA-DBS** and 87° for **SIA-DBS**. The presence of a *spiro* carbon leads to this orthogonality between the two fragments, which is at the origin of the absence of significant π-conjugation between them. This structural characteristic is the base of the present design. Additionally, in **SPA-DBS**, the angle between the acridine unit and the attached phenyl (indicated in purple in Fig. 1) is 80°, which indicates a second π-conjugation interruption at the nitrogen atom. It also changes the molecular radius (distance from the *spiro* carbon atom to the farthest carbon atom, green arrow in Fig. 1). It has been evaluated at 7.2 Å and 7.0 Å for **SPA-DBS** and **SIA-DBS**, respectively. The bond between the two phenyl rings in the IA fragment reduces the molecular radius due to a more folded structure.

For each aromatic unit, a torsion angle has been defined as the dihedral angle between the two external benzene rings of each unit (values in blue for the IA and PA units and in red for the DBS unit, Fig. 1). The acridine moiety of the PA core has a smaller torsion angle of 3.8° compared to that of the IA fragment, which presents a torsion angle of 7.2°. This is caused by the presence of a single bond between the two phenyl rings in the IA fragment, which decreases the planarity of the acridine core. For the DBS unit, the torsion angle has been measured at 8.2° and 7.2° for **SPA-DBS** and **SIA-DBS**, respectively. For both molecules, this moiety is not flat due to the presence of the central C=C bond linking the two phenyl rings, which causes some deviations from planarity.

Electrochemistry

The electrochemical properties of **SQPTZ-DBS**, **SPA-DBS** and **SIA-DBS** have been investigated by cyclic voltammetry (CV) in CH_2Cl_2 for oxidation and in DMF for reduction; potentials are given *versus* a saturated calomel electrode (SCE).

In reduction, the three compounds present a first reversible reduction wave peaking at −2.18, −2.22 and −2.17 V for **SQPTZ-DBS**, **SPA-DBS** and **SIA-DBS**, respectively (Fig. 2(A)). From their onset reduction potentials, the LUMOs were calculated to be close to −2.3 eV for the three compounds (−2.33, −2.29, and −2.35 eV for **SQPTZ-DBS**, **SPA-DBS** and **SIA-DBS**, respectively), indicating a reduction centered on the DBS core for the three compounds with only a weak effect of the *spiro*-linked donor part. This is in accordance with the molecular modelling, which shows a LUMO energy level spread out on the DBS core with only a very small contribution of the donor unit (Fig. 2(E)). This is also confirmed by the model compound **SF-DBS**, which also presents a first reversible reduction wave at −2.28 V and a LUMO energy level evaluated at −2.30 eV. Moreover, compared to its parent fluorene, one can note that the DBS unit leads to a significant decrease in the LUMO energy level by 0.49 eV, from −1.74 eV in spirobifluorene **SBF** to −2.23 eV in **SF-DBS**. This also holds true for the other couples spirophenylacridine–fluorene **SPA-F**[35]**/SPA-DBS** (−1.94 *vs.* −2.29 eV), spiroindoloacridine–fluorene **SIA-F**[36]**/SIA-DBS** (−1.88 *vs.* −2.35 eV), and

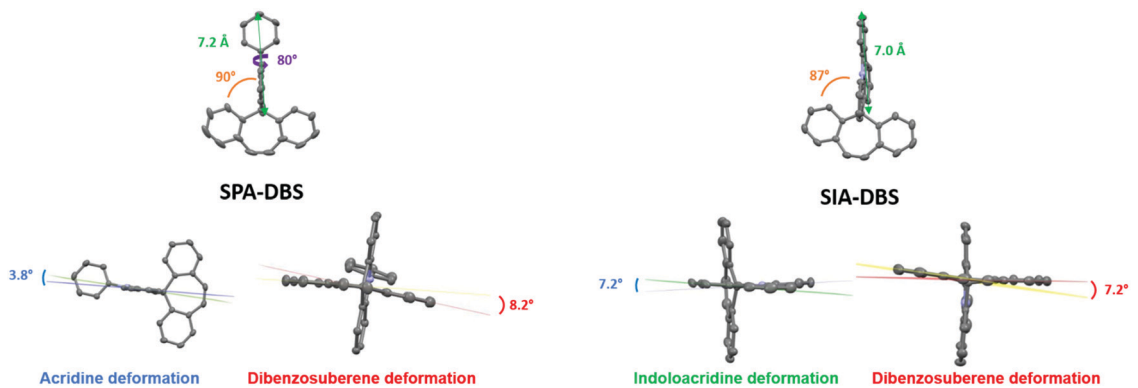

Fig. 1 Molecular structure from X-ray crystallography of **SPA-DBS** (left) and **SIA-DBS** (right) (ellipsoid probability at 50% level). Hydrogen atoms have been omitted for clarity.

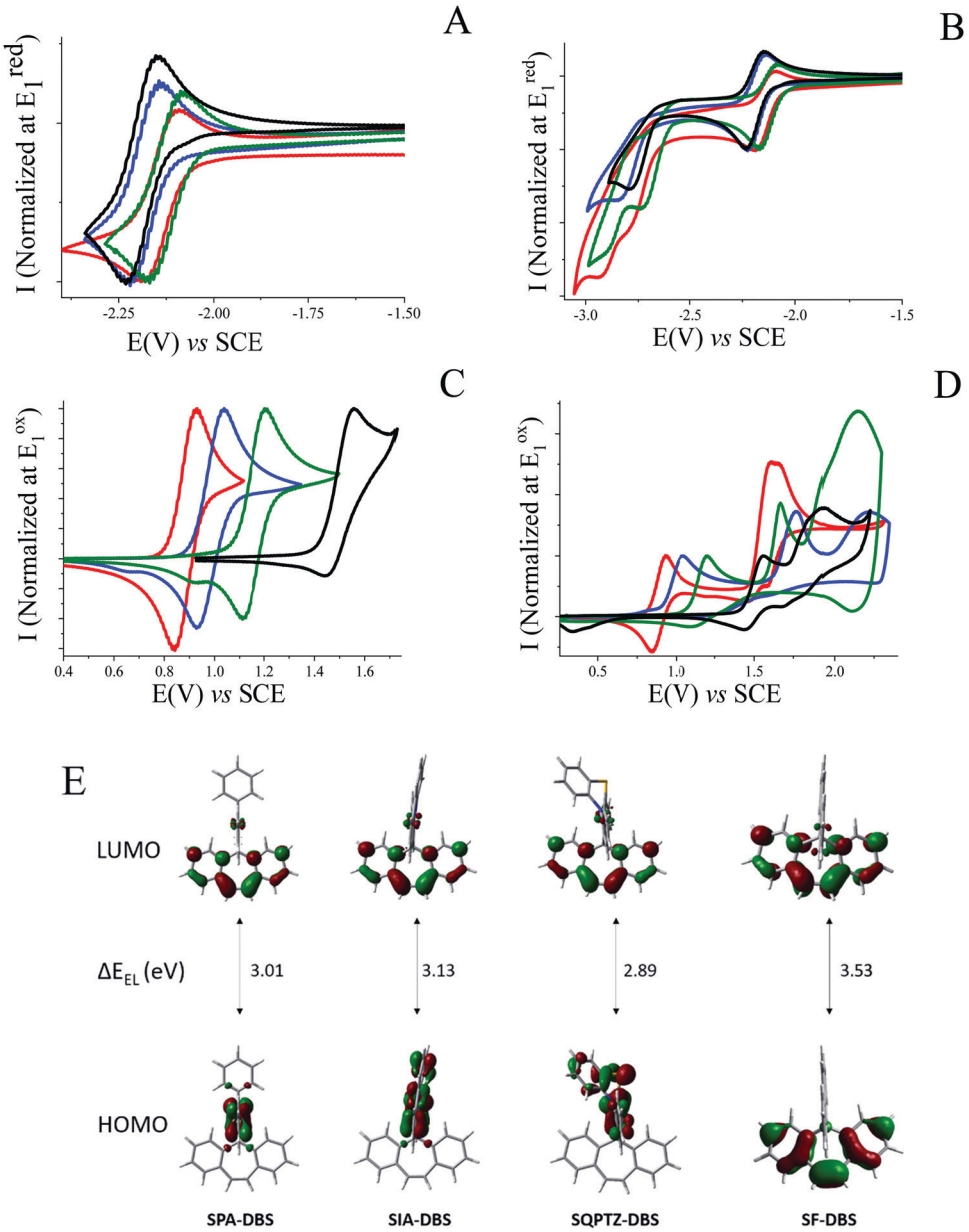

Fig. 2 Normalized cyclic voltammograms of **SQPTZ-DBS** (red lines), **SPA-DBS** (blue lines), **SIA-DBS** (green lines) and **SF-DBS** (black line) in the cathodic ((A) and (B), DMF + 0.1 M Bu_4NPF_6) or the anodic ((C) and (D), CH_2Cl_2 + 0.2 M Bu_4NPF_6) range. Sweep-rate of 100 mV s^{-1}, platinum disk (diameter 1 mm) working electrode. (E) Representations of the HOMO and LUMO obtained by DFT in B3LYP/6-311+G(d,p).

spiroquinolinophenothiazine–fluorene **SQPTZ-F**[38]**/SQPTZ-DBS** (−1.89 *vs.* −2.33 eV). This is an important consideration to allow efficient electron injection within a device.

Exploring the electrochemical behaviour up to a more negative potential reveals two additional irreversible reduction waves with maxima at −2.80 and −2.93 V for **SQPTZ-DBS** and at −2.74 and −2.90 V for **SIA-DBS** and only one irreversible reduction wave peaking at −2.86 V for **SPA-DBS** and at −2.79 V for **SF-DBS** (Fig. 2(B)). These additional reductions do not modify the reversibility of the first reduction wave indicating the stability of the different negatively charged species.

For the oxidation process, **SQPTZ-DBS**, **SPA-DBS** and **SIA-DBS** present a quasi-reversible first oxidation wave with a maximum at 0.94, 1.05 and 1.20 V, respectively (Fig. 2(C)). This first electron transfer is fully driven by the strength of the donor unit as the HOMO is exclusively spread out on this fragment (Fig. 2(E)). These results are in accordance with previously reported electrochemical data, which have highlighted the different electron-rich nature of the structurally related PA, IA and QPTZ fragments.[36–38] As the HOMO of **SF-DBS** is spread out on the DBS unit (Fig. 2(E)), this model compound displays a drastically different behaviour with a first oxidation wave that is only partially reversible and shifted to a higher

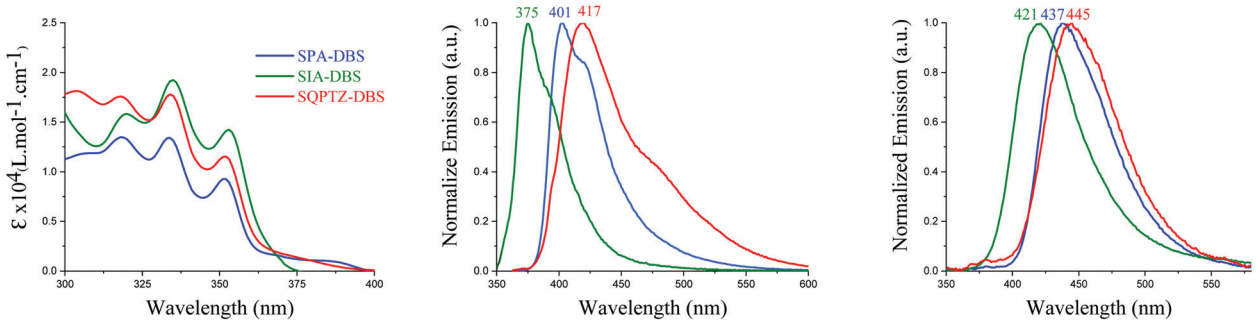

Fig. 3 Absorption (left) and emission (middle, λ_{exc} = 300 nm) in cyclohexane and emission in spin-coated thin films (right, λ_{exc} = 300 nm) of **SQPTZ-DBS** (red line), **SPA-DBS** (blue line) and **SIA-DBS** (green line).

potential (1.56 V). The HOMO energy levels were evaluated from the onset potential of the first oxidation wave at −5.22, −5.30, −5.48 and −5.83 eV for **SQPTZ-DBS**, **SPA-DBS**, **SIA-DBS** and **SF-DBS**, respectively. The second and third oxidation processes (Fig. 2(D)) are dependent on the donor unit and erase the reversibility of the first oxidation except for **SQPTZ-DBS**, where the first oxidation remains reversible even after reaching high potential values, showing the stability of the different charged species. The QPTZ building block is indeed known in the literature for the high stability of its cation radical and dication.[38] It should be noted that **SF-DBS**, when oxidized up to its second oxidation wave, is subjected to an electrodeposition process, involving carbon–carbon coupling at C2 of the fluorene units as usually observed for other fluorene based compounds.[45–47] However, no carbon–carbon coupling occurs on the DBS unit.

Photophysics

The UV-Vis absorption and emission spectra of **SQPTZ-DBS** (red line), **SPA-DBS** (blue line) and **SIA-DBS** (green line) were recorded in dilute cyclohexane solution at room temperature (Fig. 3). The optical properties are summarized in Table 1. For all these three molecules, the absorption ranges from 300 to 400 nm (Fig. 3-left), which could be assigned to π–π* transitions (see the ESI†). The TD-DFT calculations indicate that the bands experimentally found at 352–353 nm for the three compounds

Table 1 Selected electronic and physical properties of **SPA-DBS**, **SIA-DBS**, and **SQPTZ-DBS**

	SPA-DBS	**SIA-DBS**	**SQPTZ-DBS**
λ_{abs} [a] [nm (× 10^4 L mol^{-1} cm^{-1})]	318 (1.35); 334 (1.34); 352 (0.93)	320 (1.58); 335 (1.92); 353 (1.42)	318 (1.76); 334 (1.78); 352 (1.15)
$\lambda_{em\ sol}$ [ab] (nm)	401	375	417
QY_{sol} [abc]	0.12	0.12	0.02
$\lambda_{em\ film}$ [bd] (nm)	437	421	445
QY_{film} [de]	0.06	0.07	0.02
FWHM [abf] (nm)	47	38	62
$FWHM_{film}$ [bdf] (nm)	60	58	64
τ_f [ag] (at $\lambda_{em\ sol}$) [ns]	7.1 (401)	3.4 (375)	1.6 (417)
k_r [h] [ns^{-1}]	0.018	0.035	0.015
k_{nr} [h] [ns^{-1}]	0.12	0.26	0.67
E_{ox} (V *vs.* SCE) [i]	1.05, 1.76, 2.21	1.20, 1.67, 1.94, 2.15	0.94, 1.61, 1.65
E_{red} [j] (V *vs.* SCE)	−2.22, −2.86	−2.17, −2.74, −2.90*	−2.18, −2.80, −2.93
$HOMO_{exp}$ [k] (eV)	−5.30	−5.48	−5.22
$LUMO_{exp}$ [k] (eV)	−2.29	−2.35	−2.33
ΔE_{EL} [l] (eV)	3.01	3.13	2.89
$HOMO_{theo}$ [m] (eV)	−5.31	−5.59	−5.42
$LUMO_{theo}$ [m] (eV)	−1.76	−1.88	−1.90
S_1 [n] (eV)	3.33	3.54	3.30
T_d [o] (°C)	303	328	346
T_g [p] (°C)	—	105	117
T_c [p] (°C)	158	127	—
T_f [q] (°C)	243	257	210

[a] In cyclohexane at RT. [b] λ_{exc} = 300 nm. [c] Quantum yield (QY) determined with sulfate quinine in 1 M H_2SO_4 as the reference. [d] In spin-coated films. [e] QY determined in the integration sphere. [f] FWHM: full width at half maximum. [g] λ_{exc} = 310 nm. [h] $k_r = QY/\tau_f$ and $k_{nr} = (1/\tau_f) \times (1 - QY_{sol})$. [i] In dichloromethane. [j] In DMF. [k] From electrochemical data. [l] ΔE_{El} = |HOMO - LUMO|. [m] From theoretical calculations, TD-DFT B3LYP/6-311+G(d,p). [n] From the onset of the emission spectrum in cyclohexane. [o] From TGA. [p] From DSC (2nd heating cycle). [q] From DSC (1st heating cycle). *Shoulder.

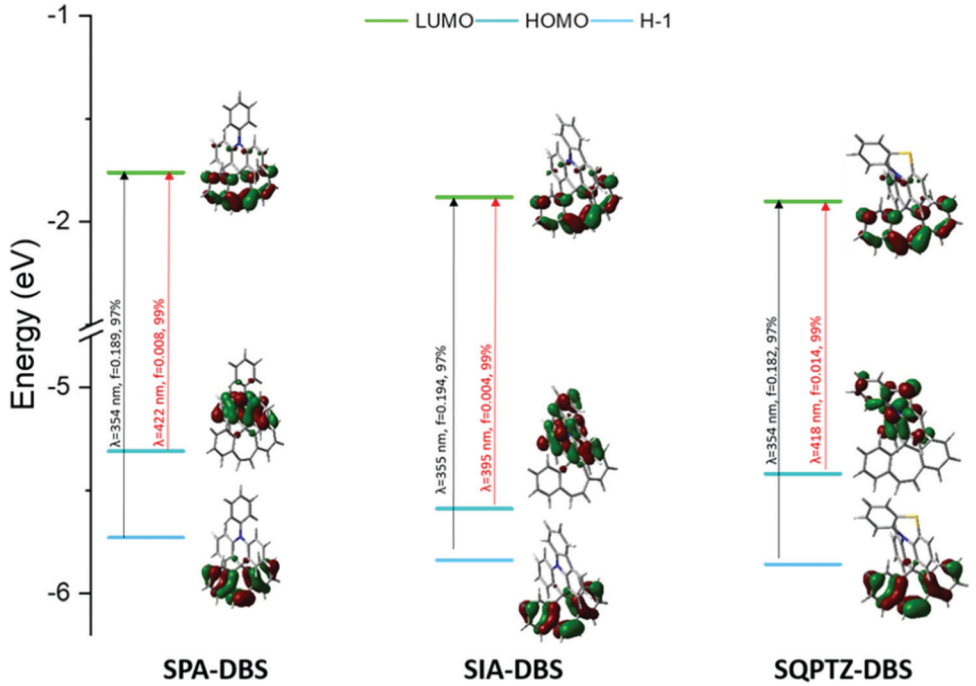

Fig. 4 Representation of the energy levels and the main molecular orbitals involved in the electronic transitions of **SPA-DBS** (left), **SIA-DBS** (middle) and **SQPTZ-DBS** (right) obtained by TD-DFT B3LYP and the 6-311+G(d, p) basis set on the geometry of S_0, shown with an isovalue of 0.04 [e $Bohr^{-3}$]$^{1/2}$ (for clarity purposes, only the main contribution for each transition is shown, details are provided in the ESI†).

are due to the HOMO−1 → LUMO transition involving orbitals both localized on the DBS part (Fig. 4). This transition is modeled at 354–355 nm for the three compounds, showing good agreement between theoretical and experimental results. Furthermore, the calculations show that the HOMO → LUMO transition is almost forbidden (oscillator strengths of 0.004–0.014 for the three compounds). Indeed, the *spiro* carbon allows good spatial separation between the HOMO localized on the donor (IA, PA or QPTZ) and the LUMO localized on the accepting DBS. In addition, it has been shown above that **SIA-DBS** displays a lower HOMO level than the two other compounds. Its weaker donor ability induces a weaker charge transfer character of the HOMO → LUMO transition compared to the PA and QPTZ counterparts. Thus, the HOMO → LUMO band of **SIA-DBS** is modeled at the lowest wavelength in the series (λ_{th} = 395, 422 and 418 nm for **SIA-DBS**, **SPA-DBS** and **SQPTZ-DBS**, respectively). For this reason, this band, in the UV-Vis absorption spectrum, is hidden by the HOMO−1 → LUMO band in the case of **SIA-DBS** but can be detected as a shoulder for **SPA-DBS** and **SQPTZ-DBS**.

The emission properties of these three molecules were then determined in cyclohexane (Fig. 3, middle). The three compounds display fluorescence features in the deep blue region with a red shift of the maximum emission, from 375 nm for **SIA-DBS**, to 401 nm for **SPA-DBS** and to 417 nm for **SQPTZ-DBS** (corresponding S_1 values are 3.54, 3.33 and 3.30 eV). Thus, opposite to their absorption spectra, which were similar, the emission spectra appear to be very different with a 42 nm red shift between **SIA-DBS** and **SQPTZ-DBS**. This can be assigned to electronic and structural features. Indeed, the more electron rich-nature of the QPTZ fragment induces a stronger photo-induced intramolecular charge transfer (ICT), which causes a red shift. In addition, due to the presence of the sulphur bridge, the QPTZ fragment is significantly more flexible than the rigid IA unit, causing more important geometry modification between S_0 and S_1, which in turn leads to a red shift of the emission. Compared to the fluorene-based counterparts, **SPA-F**, **SIA-F** and **SQPTZ-F** previously reported in the literature (see structures in the ESI†), which possess an emission wavelength at 345, 361 and 417 nm, respectively,[35,36,38,48] one can note that for the DBS compounds, an extension of the conjugation pathway, induced by the presence of the double bond between the two phenyl rings, causes a significant red shift of the emission maxima. This allows the present DBS-based fluorophores to achieve an emission in the deep-blue region.

The quantum yields of both **SIA-DBS** and **SPA-DBS** are measured at 0.12 whereas that of **SQPTZ-DBS** is 6 times lower, 0.02, in accordance with a more important ICT in the latter (see below solvatochromic experiments). This is expected in view of the very low oscillator strength arising from the spatial separation of the electron-rich and the electron-poor fragments, which promotes a vanishingly small transition dipole moment between the S_1 and S_0 states. The three compounds exhibit single lifetimes, dependent on the donor unit. Thus, **SPA-DBS** displays a long lifetime of 7.1 ns, whereas those of **SIA-DBS** and **SQPTZ-DBS** are significantly reduced (3.4 and 1.6 ns, respectively). The analysis of the radiative (k_r) and the non-radiative (k_{nr}) constants provides interesting data on the deexcitation of

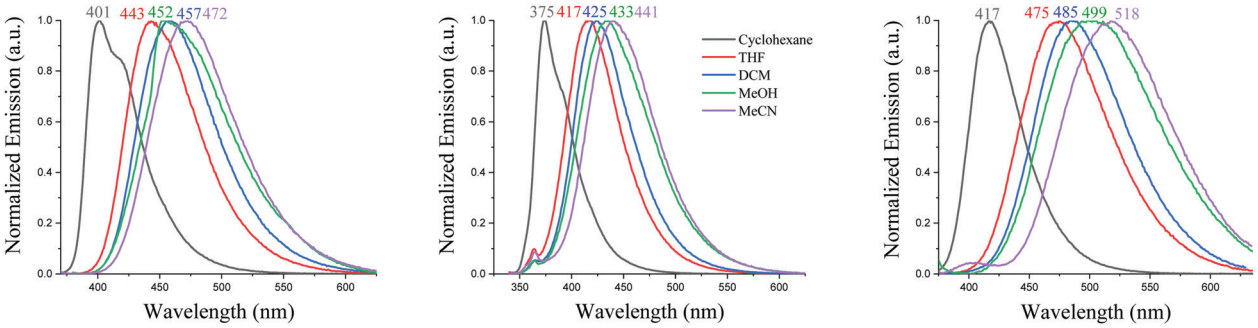

Fig. 5 Emission spectra in different solvents of **SPA-DBS** (left), **SIA-DBS** (middle) and **SQPTZ-DBS** (right), λ_{exc} = 330 nm.

excited states. Indeed, for the three compounds, the k_r values are very weak, in accordance with the small oscillator strength observed between the S_0 and S_1 states. The k_{nr} of **SQPTZ-DBS** is the highest in the series, six times higher than that of **SPA-DBS** (0.67 and 0.12 ns^{-1}, respectively). Their k_r values are almost identical (0.018 and 0.015 ns^{-1} respectively), which shows that the presence of the sulphur bridge in **SQPTZ-DBS** and the resulting flexibility induced, leads to an increase of the vibrational deactivation pathways (and an increase in the ISC as previously reported[37]), leading to a decrease of the quantum yield. This is in accordance with the conclusions mentioned above in terms of wavelength emission. Thus, the sulphur bridge of the QPTZ fragment (which is a building unit only recently investigated for organic electronic applications[37–39]) leads to very appealing electrochemical properties (a high HOMO and stability of the cation radical), but increases the non-radiative pathways. It is finally important to mention that no phosphorescence contribution is observed at 77 K in Me-THF for all compounds. This is a different behaviour compared to their fluorene analogues and hence assigned to the DBS fragment.

Solvatochromic experiments allow visualizing the strength of the three donor units through the intensity of the ICT occurring in these systems, Fig. 5. For the three compounds, there is a significant red shift from apolar cyclohexane to highly polar MeCN, 66 nm for **SIA-DBS**, 71 nm for **SPA-DBS** and 101 nm for **SQPTZ-DBS**. The red shift reflects a more intense ICT and follows the strength of the donor highlighted in the electrochemical part. In the case of **SIA-DBS**, the presence of a small band at low wavelength is detected as soon as the polarity of the solvent increased. This band is assigned to a locally excited state as it is not dependent on the polarity of the medium and recorded at *ca.* 363 nm, almost identical to the maximum observed in cyclohexane (375 nm, Fig. 5). Such behaviour is sometimes detected for donor/acceptor compounds.[36]

The differences ($\Delta\mu$) between the dipole moment at the ground state (μ) and at the first excited state (μ^*) have been evaluated using the Lippert–Mataga formalism. $\Delta\mu$ of 16.3, 15.9 and 17.9 D have been measured (the dipole moments at the ground state have been obtained by DFT calculations, 2.2, 0.6 and 1.4 D) for **SPA-DBS**, **SIA-DBS** and **SQPTZ-DBS**, respectively (see the ESI†). These $\Delta\mu$ data reflect the different polarities of the three fluorophores in their excited states (μ^* = 18.5, 16.5 and 19.3 D, respectively). The solvatochromic effect (Fig. 5) and the corresponding high $\Delta\mu$ observed for **SPA-DBS**, **SIA-DBS** and **SQPTZ-DBS** are indicative of a significant photoinduced ICT. Thus, one can note that the QPTZ fragment provides the highest $\Delta\mu$ due to its electron-rich behaviour being stronger than those of the PA and IA analogues **SPA-DBS** and **SIA-DBS**.

Solid state fluorescence spectra have finally been recorded before any OLED application. From solution to film, there is a

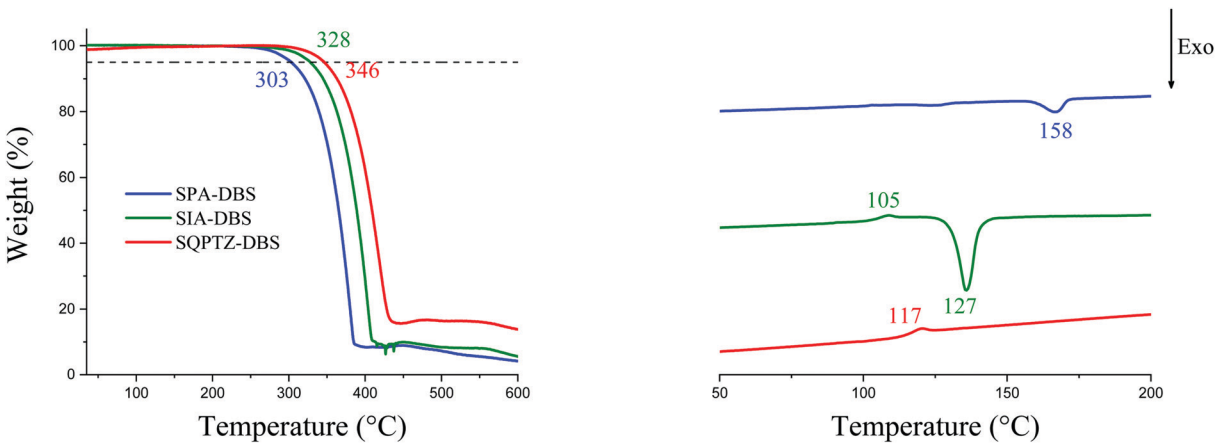

Fig. 6 TGA (left) and DSC (right, 2nd heating cycle only) of **SPA-DBS** (blue lines), **SIA-DBS** (green lines) and **SQPTZ-DBS** (red lines).

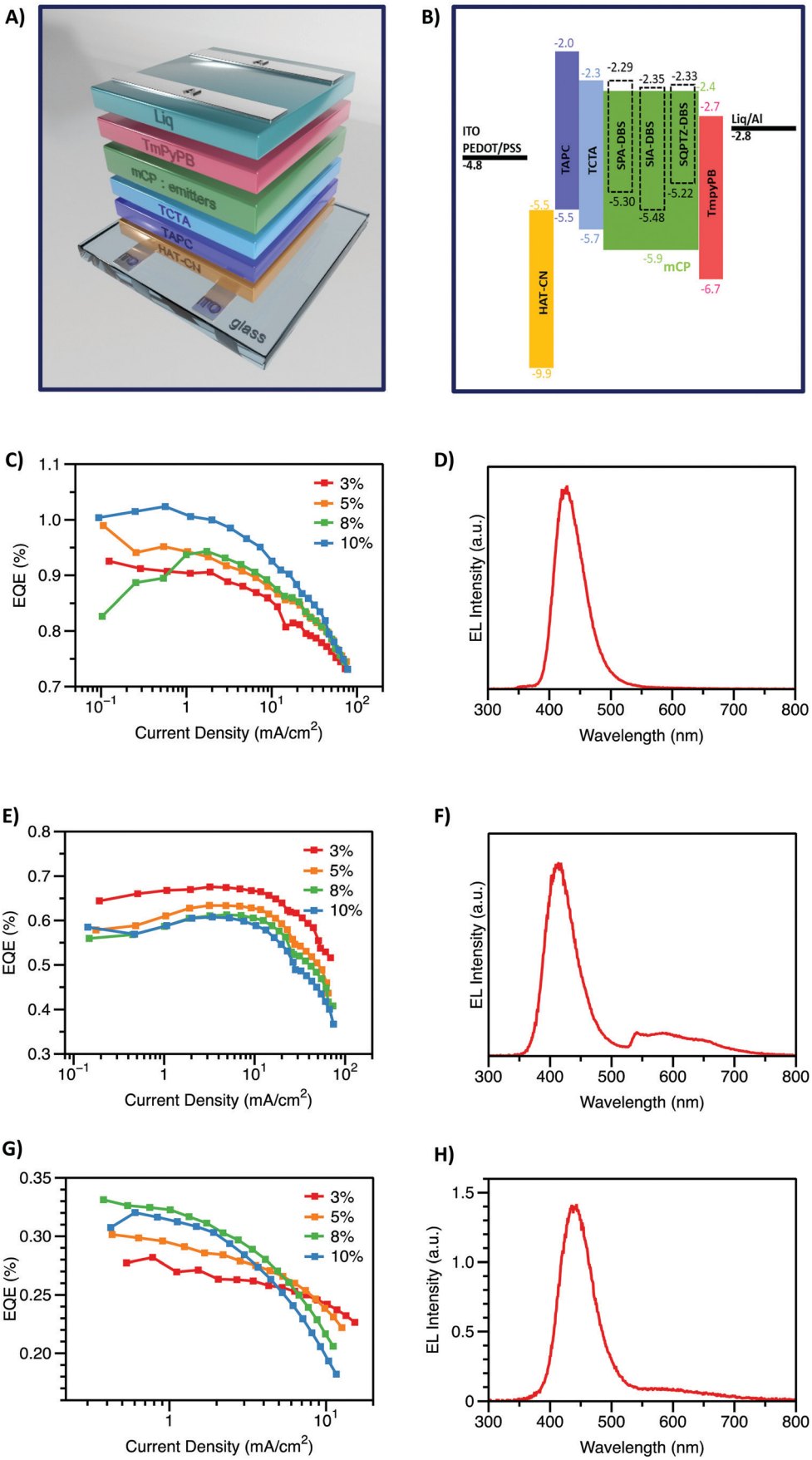

Fig. 7 Device structure (A), energy levels diagram (B). Electroluminescence spectra and EQE *vs.* current density of **SPA-DBS** (C) and (D), **SIA-DBS** (E) and (F) and **SQPTZ-DBS** (G) and (H).

Table 2 Best OLED performances using **SPA-DBS**, **SIA-DBS** and **SQPTZ-DBS** as emitters with different percentages of doping and mCP as the host material

Host	Dopant	V_{on}[a] (V)	CE_{max} (cd A^{-1})	EQE_{max} (%)	λ_{max} (nm)	FWHM (nm)	CIE[b] (x, y)
mCP	**SPA-DBS** (10%)	4.0	0.439	1.024	428	55	(0.16, 0.04)
	SIA-DBS (3%)	3.5	0.668	0.676	414	60	(0.24, 0.14)
	SQPTZ-DBS (8%)	5.1	0.205	0.331	442	61	(0.18, 0.10)

[a] Recorded at a luminance of 1 cd m^{-2}. [b] Measured at a driving current density of 5 mA cm^{-2}.

red shift detected for the three emitters, 46 nm for **SIA-DBS**, 36 nm for **SPA-DBS** and 28 nm for **SQPTZ-DBS** due to the different environments (Fig. 3, right). However, the emission remains in the deep-blue region with maxima at 421, 437 and 445 nm, respectively, which is highly beneficial for the targeted application (see below).

Thermal properties

Before any possible OLED application, the thermal properties should be evaluated by means of thermogravimetric analyses (TGA) and differential scanning calorimetry (DSC), Fig. 6. In the present case, the three emitters possess a high decomposition temperature T_d (5% mass loss), above 300 °C. More importantly, **SQPTZ-DBS** presents a higher glass transition temperature T_g (117 °C determined by DSC during the 2nd heating run, between 20 and 260 °C) compared to **SIA-DBS**, which presents a T_g detected at 105 °C. It is important to note that no T_g values were observed under the same conditions for **SPA-DBS**. Both high T_g and high T_d parameters are important to achieve highly stable devices. Thus, incorporation of a sulfur atom in **SQPTZ-DBS** is beneficial for further OLED applications in terms of thermal properties. **SPA-DBS** and **SIA-DBS** present a crystallization temperature T_c at *ca.* 158 °C and 127 °C respectively which is suppressed in the QPTZ based compounds. As amorphous materials are highly desired in this field, this is an important characteristic of the QPTZ fragment.

OLED devices

Finally, the compounds were incorporated as emitters in OLED devices. As shown in Fig. 7, the optimal device configuration was ITO/HAT-CN (10 nm)/TAPC (40 nm)/TCTA (10 nm)/mCP:emitters (x%, 20 nm)/TmPyPB (40 nm)/Liq (2 nm)/Al (120 nm). The concentration of the emitter in the emissive layer was evaluated between 3 and 10% (see Fig. S15–S17, ESI†).

The electroluminescence (EL) spectra, recorded at a current density of 5 mA cm^{-2}, appear to be very different and dependent on the electron-rich fragment (Fig. 7(D), (F) and (H)). Indeed, in the case of both **SIA-DBS** and **SQPTZ-DBS**, a large band between 500 and 700 nm is observed, in addition to the blue contribution respectively observed at 414 and 442 nm. Such a band in the green region has been the subject of intense research studies in the field of blue OLEDs in order to find its origin (π–π interactions, keto defect, *etc.*).[17,49–51] Due to this parasite band, the CIE coordinates, respectively measured at (0.24, 0.14) and (0.18, 0.10) for **SIA-DBS** and **SQPTZ-DBS** do not fit with the chromatic standards mentioned above. However, **SPA-DBS** does not present this parasite green emission band and its EL spectrum only displays the blue contribution at 428 nm, very similar to that recorded in solid thin films, at 437 nm (Fig. 3, right). This device possesses a good colour purity as its full width at half-maximum (FWHM) is estimated to be 55 nm, almost identical to that measured in thin-solid films (60 nm, Table 1). The difference observed between the three compounds may arise from the extended cores of IA and QPTZ *vs.* PA, which may favour π–π stacking. Thus, the CIE coordinates of the **SPA-DBS** based device (0.16, 0.04) appear to be very interesting for displays, with a particularly low CIEy value of 0.04. The current density *versus* EQE plots for these devices are presented in Fig. 7 and the device performance is summarized in Table 2 (detailed performance is shown in the ESI†). These devices display turn-on voltages (V_{on} at 1 Cd cm^{-2}) ranging from 3.5 to 5.1 V in the same range as those obtained with the best fluorescent violet OLEDs reported to date in the literature (3.6–3.8 V).[29] This is directly related to the presence of electron-rich units in these structures. These values appear nevertheless a little bit high due to the low concentration of emitters in the large bandgap material mCP. In terms of performance, the highest EQE is measured for **SPA-DBS** with an EQE of 1.02% (10% emitter). Thus, the performance of **SPA-DBS** based OLEDs with a V_{on} of 4 V, an EQE of *ca.* 1% and CIE coordinates of (0.16, 0.04) is a first step towards the development of violet DBS based emitters with low CIEy. These CIE coordinates closely approach the ITU-R Recommendation BT.2020 (Rec. 2020) standard of (0.131, 0.046).[29]

Conclusion

To conclude, we report in this work the synthesis, the physicochemical properties and the application of deep blue emitters constructed using the dibenzosuberene molecular fragment in OLEDs. As the charge injection is particularly important in deep-blue emission, electron-rich units, namely *N*-phenylacridine, indoloacridine and quinolinophenothiazine, have been connected to the DBS core. The resulting organic materials display similar LUMO levels lying at *ca.* −2.30 eV and different HOMO levels driven by the donor unit located between −5.22 and −5.48 eV. The *spiro*-configuration allows maintaining high T_g and T_d in accordance with the OLED application. **SPA-DBS** displays a deep-blue emission with CIE coordinates of (0.16, 0.04), reaching an EQE of *ca.* 1% and possessing a very low CIEy coordinate of 0.04. This CIEy coordinate fits the NSTC, ITU and EBU standards. This work not only reports a deep blue emitter for an OLED but also sheds light on interesting properties displayed by the DBS fragment, such as its low LUMO energy level, *ca.* −2.3 eV, which is significantly lower compared to that of its counterpart fluorene. This particularity can be advantageously used in further designs to favour the electron injection in electronic devices.

Conflicts of interest

There are no conflicts to declare.

Acknowledgements

The authors would like to thank the ANR (SPIROQUEST, no. 19-CE05-0024) for financial support of this project, and the Agence de l'Environnement et de la Maitrise de l'Energie (ADEME, Bruno Lafitte) for a PhD grant (CB, EcoElec Project). We would like to thank Dr Maxime Romain who have initiated dibenzosuberene compounds in the group, GENCI (No. AD0100805032R1) for computing time and the CRMPO (Rennes) for mass analysis. The authors thank Dr J. F. Bergamini (Rennes) for the TOC material.

References

1 G. Hong, X. Gan, C. Leonhardt, Z. Zhang, J. Seibert, J. M. Busch and S. Bräse, A brief history of OLEDs–emitter development and industry milestones, *Adv. Mater.*, 2021, **33**, 2005630.
2 R. Mertens, *The OLED Handbook: A Guide to OLED Technology, Industry & Market*, 2019.
3 Y.-K. Qu, Q. Zheng, J. Fan, L.-S. Liao and Z.-Q. Jiang, Spiro compounds for organic light-emitting diodes, *Acc. Mater. Res.*, 2021, **2**, 1261.
4 C. W. Tang and S. A. Vanslike, Organic electroluminescent diodes, *Appl. Phys. Lett.*, 1987, **51**, 913.
5 C. Poriel and J. Rault-Berthelot, Blue single-layer organic light-emitting diodes using fluorescent materials: A molecular design view point, *Adv. Funct. Mater.*, 2020, **30**, 1910040.
6 J. R. Sheats, H. Antoniadis, M. Hueschen, W. Leonard, J. Miller, R. Moon, D. Roitman and A. Stocking, Organic electroluminescent devices, *Science*, 1996, **273**, 884.
7 R. H. Friend, R. W. Gymer, A. B. Holmes, J. H. Burroughes, R. N. Marks, C. Taliani, D. D.-C. Bradley, D. A. Dos Santos, J. L. Bredas, M. Lögdlund and W. R. Salaneck, Electroluminescence in conjugated polymers, *Nature*, 1999, **397**, 121.
8 M. A. Baldo, D. F. O'Brien, Y. You, A. Shoustikov, S. Sibley, M. E. Thompson and S. R. Forrest, Highly efficient phosphorescent emission from organic electroluminescent devices, *Nature*, 1998, **395**, 151.
9 Y. Tao, C. Yang and J. Qin, Organic host materials for phosphorescent organic light-emitting diodes, *Chem. Soc. Rev.*, 2011, **40**, 2943.
10 K. S. Yook and J. Y. Lee, Small Molecule Host Materials for Solution Processed Phosphorescent Organic Light-Emitting Diodes, *Adv. Mater.*, 2014, **26**, 4218.
11 C. Poriel and J. Rault-Berthelot, Structure–property relationship of 4-substituted-spirobifluorenes as hosts for phosphorescent organic light emitting diodes: An overview, *J. Mater. Chem. C*, 2017, **5**, 3869.
12 C. Poriel and J. Rault-Berthelot, Designing host materials for the emissive layer of single-layer phosphorescent organic light-emitting diodes: Toward simplified organic devices, *Adv. Funct. Mater.*, 2021, **31**, 2010547.
13 Q. Wang, F. Lucas, C. Quinton, Y.-K. Qu, J. Rault-Berthelot, O. Jeannin, S.-Y. Yang, F.-C. Kong, S. Kumar, L.-S. Liao, C. Poriel and Z.-Q. Jiang, Evolution of pure hydrocarbon hosts: Simpler structure, higher performance and universal application in RGB phosphorescent organic light-emitting diodes, *Chem. Sci.*, 2020, **11**, 4887.
14 A. Endo, M. Ogasawara, A. Takahashi, D. Yokoyama, Y. Kato and C. Adachi, Thermally activated delayed fluorescence from Sn^{4+} – porphyrin complexes and their application to organic light emitting diodes—a novel mechanism for electroluminescence, *Adv. Mater.*, 2009, **21**, 4802.
15 M. Y. Wong and E. Zysman-Colman, Purely organic thermally activated delayed fluorescence materials for organic light-emitting diodes, *Adv. Mater.*, 2017, **29**, 1605444.
16 Y. Zhang, G. Cheng, Y. Zhao, J. Hou, S. Liu, S. Tang and Y. Ma, Organic pure-blue-light-emitting devices based on terfluorenes compounds, *Appl. Phys. Lett.*, 2005, **87**, 241112.
17 C. Poriel, N. Cocherel, J. Rault-Berthelot, L. Vignau and O. Jeannin, Incorporation of spiroxanthene units in blue-emitting oligophenylene frameworks: A new molecular design for OLED applications, *Chem. Eur. J.*, 2011, **17**, 12631.
18 N. Cocherel, C. Poriel, L. Vignau, J.-F. Bergamini and J. Rault-Berthelot, Dispiroxanthene-indenofluorene: A new blue emitter for nondoped organic light emitting diode applications, *Org. Lett.*, 2010, **12**, 452.
19 H. L. Lee, W. J. Chung and J. Y. Lee, Narrowband and pure violet organic emitter with a full width at half maximum of 14 nm and y color coordinate of below 0.02, *Small*, 2020, **16**, 1907569.
20 Y. Yuan, Y. Hu, Y.-X. Zhang, J.-D. Lin, Y.-K. Wang, Z.-Q. Jiang, L.-S. Liao and S.-T. Lee, Over 10% EQE near-infrared electroluminescence based on a thermally activated delayed fluorescence emitter, *Adv. Funct. Mater.*, 2017, **27**, 1700986.
21 M. Maclean, L. E. Murdoch, S. J. MacGregor and J. G. Anderson, Sporicidal effects of high-intensity 405 nm visible light on endospore-forming bacteria, *Photochem. Photobiol.*, 2013, **89**, 120.
22 J.-H. Lee, C.-H. Chen, P.-H. Lee, H.-Y. Lin, M.-k Leung, T.-L. Chiu and C.-F. Lin, Blue organic light-emitting diodes: Current status, challenges, and future outlook, *J. Mater. Chem. C*, 2019, **7**, 5874.
23 Y. Wang, J. H. Yun, L. Wang and J. Y. Lee, High triplet energy hosts for blue organic light-emitting diodes, *Adv. Funct. Mater.*, 2020, **31**, 2008332.
24 X. Yang, X. Xu and G. Zhou, Recent advances of the emitters for high performance deep-blue organic light-emitting diodes, *J. Mater. Chem. C*, 2015, **3**, 913.
25 A. Monkman, Why do we still need a stable long lifetime deep blue OLED Emitter?, *ACS Appl. Mater. Interfaces*, 2022, **14**, 20463–20467.
26 C. Poriel, J. Rault-Berthelot and Z.-Q. Jiang, Are pure hydrocarbons the future of host materials for blue phosphorescent organic light-emitting diodes?, *Mater. Chem. Front.*, 2022, **6**, 1246–1252.
27 C. Poriel and J. Rault-Berthelot, Pure hydrocarbons: An efficient molecular design strategy for the next generation of host materials for phosphorescent organic light-emitting diodes, *Acc. Mater. Res.*, 2022, **3**, 379.
28 F. Dumur, Deep-blue organic light-emitting diodes: From fluorophores to phosphors for high-efficiency devices,

Advanced Surface Engineering Materials, Scrivener Publishing, 2016, p. 561.

29 S. N. Zou, X. Chen, S. Y. Yang, S. Kumar, Y. K. Qu, Y. J. Yu, M. K. Fung, Z. Q. Jiang and L. S. Liao, Efficient violet organic light-emitting diodes with CIE*y* of 0.02 Based on Spiro Skeleton, *Adv. Opt. Mater.*, 2020, **8**, 2001074.

30 Y. Wei and C.-T. Chen, Doubly ortho-linked *cis*-4,4′-bis(diarylamino)stilbene/fluorene hybrids as efficient non-doped, sky-blue fluorescent materials for optoelectronic applications, *J. Am. Chem. Soc.*, 2007, **129**, 7478.

31 J.-H. Jou, Y.-T. Su, M.-T. Hsiao, H.-H. Yu, Z.-K. He, S.-C. Fu, C.-H. Chiang, C.-T. Chen, C.-h Chou and J.-J. Shyue, Solution-process-feasible deep-red phosphorescent emitter, *J. Phys. Chem. C*, 2016, **120**, 18794.

32 C.-T. Chen, Y. Wei, J.-S. Lin, M. V.-R. K. Moturu, W.-S. Chao, Y.-T. Tao and C.-H. Chien, Doubly ortho-linked quinoxaline/diphenylfluorene hybrids as bipolar, fluorescent chameleons for optoelectronic applications, *J. Am. Chem. Soc.*, 2006, **128**, 10992.

33 M. Romain, D. Tondelier, B. Geffroy, O. Jeannin, E. Jacques, J. Rault-Berthelot and C. Poriel, Donor/acceptor dihydroindeno[1,2-*a*]fluorene and dihydroindeno[2,1-*b*]fluorene: Towards new families of organic semiconductors, *Chem. Eur. J.*, 2015, **21**, 9426.

34 M. Romain, D. Tondelier, O. Jeannin, B. Geffroy, J. Rault-Berthelot and C. Poriel, Properties modulation of organic semi-conductors based on a donor-spiro-acceptor (D-spiro-A) molecular design: New host materials for efficient sky-blue PhOLEDs, *J. Mater. Chem. C*, 2015, **3**, 97010.

35 F. Lucas, C. Quinton, S. Fall, T. Heiser, D. Tondelier, B. Geffroy, N. Leclerc, J. Rault-Berthelot and C. Poriel, Universal host materials for red, green and blue high-efficiency single-layer phosphorescent organic light-emitting diodes, *J. Mater. Chem. C*, 2020, **8**, 16354.

36 S. Thiery, D. Tondelier, B. Geffroy, O. Jeannin, J. Rault-Berthelot and C. Poriel, Modulation of the physicochemical properties of donor–spiro–acceptor derivatives through donor unit planarisation: Phenylacridine *versus* indoloacridine—new hosts for green and blue phosphorescent organic light-emitting diodes (PhOLEDs), *Chem. Eur. J.*, 2016, **22**, 10136.

37 C. Poriel, J. Rault-Berthelot, S. Thiery, C. Quinton, O. Jeannin, U. Biapo, B. Geffroy and D. Tondelier, 9*H*-quinolino[3,2,1-*k*]phenothiazine: A new electron-rich fragment for organic electronics, *Chem. Eur. J.*, 2016, **22**, 17930.

38 F. Lucas, D. Tondelier, B. Geffroy, T. Heiser, O. A. Ibraikulov, C. Quinton, C. Brouillac, N. Leclerc, J. Rault-Berthelot and C. Poriel, Quinolinophenothiazine as electron rich fragment for RGB Single-layer phosphorescent organic light-emitting diodes, *Mater. Chem. Front.*, 2021, **5**, 8066.

39 C. Quinton, L. Sicard, O. Jeannin, N. Vanthuyne and C. Poriel, Confining nitrogen inversion to yield enantiopure quinolino[3,2,1-*k*]phenothiazine derivatives, *Adv. Funct. Mater*, 2018, **28**, 1803140.

40 T. P.-I. Saragi, T. Spehr, A. Siebert, T. Fuhrmann-Lieker and J. Salbeck, Spiro compounds for organic optoelectronics, *Chem. Rev.*, 2007, **107**, 1011.

41 L.-H. Xie, J. Liang, J. Song, C.-R. Yin and W. Huang, Spirocyclic aromatic hydrocarbons (SAHs) and their synthetic methodologies, *Curr. Org. Chem.*, 2010, **14**, 2169.

42 S. Liu, D. Xia and M. Baumgarten, Rigidly-fused spiro-conjugated π-systems, *ChemPlusChem*, 2021, **21**, 36.

43 C. Poriel, L. Sicard and J. Rault-Berthelot, New generations of spirobifluorene regioisomers for organic electronics: Tuning electronic properties with the substitution pattern, *Chem. Commun.*, 2019, **55**, 14238.

44 C. Poriel and J. Rault-Berthelot, Dihydroindenofluorene positional isomers, *Acc. Chem. Res.*, 2018, **51**, 1818.

45 Y. Ferrand, C. Poriel, P. Le Maux, J. Rault-Berthelot and G. Simonneaux, Asymmetric heterogeneous carbene transfer catalyzed by optically active ruthenium spirobifluorenylporphyrin polymers, *Tetrahedron: Asymmetry*, 2005, **16**, 1463.

46 C. Poriel, Y. Ferrand, P. Le Maux, J. Rault-Berthelot and G. Simonneaux, Organic cross-linked electropolymers as supported oxidation catalysts: Poly((tetrakis(9,9′-spirobifluorenyl)porphyrin)manganese) films, *Inorg. Chem.*, 2004, **43**, 5086.

47 C. Poriel, Y. Ferrand, P. Le Maux, C. Paul-Roth, G. Simonneaux and J. Rault-Berthelot, Anodic oxidation and physicochemical properties of various porphyrin-fluorenes or -spirobifluorenes: Synthesis of new polymers for heterogeneous catalytic reactions, *J. Electroanal. Chem.*, 2005, **583**, 92.

48 F. Lucas, O. A. Ibraikulov, C. Quinton, L. Sicard, T. Heiser, D. Tondelier, B. Geffroy, N. Leclerc, J. Rault-Berthelot and C. Poriel, Spirophenylacridine-2,7-(diphenylphosphineoxide)-fluorene: A bipolar host for high-efficiency single-layer blue phosphorescent organic light-emitting diodes, *Adv. Opt. Mater.*, 2020, **8**, 1901225.

49 K. L. Chan, M. Sims, S. I. Pascu, M. Ariu, A. B. Holmes and D. D.-C. Bradley, Understanding the nature of the states responsible for the green emission in oxidized poly(9,9-dialkylfluorene)s: Photophysics and structural studies of linear dialkylfluorene/fluorenone model compounds, *Adv. Funct. Mater.*, 2009, **19**, 2147.

50 A. C. Grimsdale, In search of stable blue emission from phenylene-based conjugated polymers, *Curr. Org. Chem.*, 2010, **14**, 2196.

51 N. Cocherel, C. Poriel, J. Rault-Berthelot, F. Barrière, N. Audebrand, A. M.-Z. Slawin and L. Vignau, New 3π-2 spiro ladder-type phenylene materials: Synthesis, physicochemical properties and applications in OLEDs, *Chem. Eur. J.*, 2008, **14**, 11328.